

NUMERICAL MODELLING OF THE SEPARATION OF COMPLEX SHAPED PARTICLES IN AN OPTICAL BELT SORTER USING A DEM–CFD APPROACH AND COMPARISON WITH EXPERIMENTS

CHRISTOPH PIEPER¹, GEORG MAIER², FLORIAN PFAFF³, HARALD KRUGGEL-EMDEN⁴, ROBIN GRUNA², BENJAMIN NOACK³, SIEGMAR WIRTZ¹, VIKTOR SCHERER¹, THOMAS LÄNGLE², UWE D. HANEBECK³ AND JÜRGEN BEYERER²

¹Department of Energy Plant Technology
Ruhr-University Bochum
Universitätsstraße 150, 44780 Bochum, Germany
e-mail: pieper@leat.rub.de, web page: <https://www.leat.rub.de/>

²Fraunhofer Institute of Optronics,
System Technologies and Image Exploration
Fraunhoferstraße 1, 76131 Karlsruhe, Germany

³Intelligent Sensor-Actuator-Systems Laboratory
Karlsruhe Institute of Technology
Adenauerring 2, 76131 Karlsruhe, Germany

⁴Mechanical Process Engineering and Solids Processing
Technical University Berlin
Ernst-Reuter-Platz 1, 10587 Berlin, Germany

Key words: Optical sorting, DEM, CFD, Complex shaped particles

Abstract. In the growing field of bulk solids handling, automated optical sorting systems are of increasing importance. However, the initial sorter calibration is still very time consuming and the precise optical sorting of many materials still remains challenging. In order to investigate the impact of different operating parameters on the sorting quality, a numerical model of an existing modular optical belt sorter is presented in this study. The sorter and particle interaction is described with the Discrete Element Method (DEM) while the air nozzles required for deflecting undesired material fractions are modelled with Computation Fluid Dynamics (CFD). The correct representation of the resulting particle–fluid interaction is realized through a one–way coupling of the DEM with CFD. Complex shaped particle clusters are employed to model peppercorns also used in experimental investigations. To test the correct implementation of the utilized models, the particle mass flow within the sorter is compared between experiment and simulation. The particle separation results of the developed numerical model of the optical sorting system are compared with matching experimental investigations. The findings show that the numerical model is able to predict the sorting quality of the optical sorting system with reasonable accuracy.

1 INTRODUCTION

The handling and sorting of bulk solids is of increasing importance due to continuously growing material streams [1]. Automated optical sorters can be used in addition to conventional separating processes like screens [2], which separate the material depending on physical properties like the size. Optical sorters are employed in a variety of industrial applications and are able to separate agricultural products or particulate chemical/pharmaceutical substances based on optical criteria [3]. The material stream is transported and isolated by chutes, slides or vibrating feeders and bypasses an optical sensor, before the bulk solids are separated into at least two fractions by pneumatic air nozzles. The nozzles are triggered based on the optical properties of the material.

Studies investigating the influence of optical sorter design and operation on sorting quality are still relatively scarce. De Jong and Harbeck [4] investigated the maximum throughput of an optical sorter based on different particle sizes in 2005, with the conclusion that the separation efficiency decreases if a minimum distance between adjacent particles is below a certain threshold. Pascoe et al. [5] developed a model for predicting the efficiency of their sorting system depending on the belt loading and the number of particles to be ejected. In a further study [6], the authors investigated the influence of special particle distribution on the sorting efficiency with the help of a Monte Carlo simulation. Particle ejection by compressed air has been investigated with a coupled DEM–CFD approach by Fitzpatrick et al. [7]. However, only the ejection stage with the resulting particle–fluid interaction was analyzed. In a previous study, we have shown that the DEM is able to correctly model the effect of different operating parameters on particle movement within an optical sorter [8].

In this study, a modular optical belt sorter consisting of a vibrating feeder, conveyor belt, compressed air nozzles for particle separation and a particle container is modelled with a coupled DEM–CFD approach. A sorting task is defined and an experiment on a fully operational modular sorting system is conducted. The particle separation results of the experiment are compared with those of the corresponding numerical setup.

2 METHODOLOGY

2.1 DEM-CFD approach

The Discrete Element Method (DEM) [9] is used to describe the modular optical belt sorter as well as the bulk solids investigated in this study. The DEM allows the detailed analysis of particle–particle and particle–wall interactions within the sorting system. Newton’s and Euler’s equations of motion are used to calculate the translational and rotational motion of every particle and can be written as

$$m_i \frac{d^2 \vec{x}_i}{dt^2} = \vec{F}_i^c + \vec{F}_i^g + \vec{F}_i^{pf}, \quad (1)$$

$$\hat{I}_i \frac{d\vec{\omega}_i}{dt} + \vec{\omega}_i \times (\hat{I}_i \vec{\omega}_i) = \Lambda_i^{-1} \vec{M}_i, \quad (2)$$

where m_i is the particle mass, $d^2 \vec{x}_i / dt^2$ the particle acceleration, \vec{F}_i^c the contact force, \vec{F}_i^g the gravitational force and \vec{F}_i^{pf} is the particle–fluid force. The second equation gives the angular

acceleration $d\vec{W}_i/dt$ as a function of the angular velocity \vec{W}_i , the external moment resulting from the contact forces \vec{M}_i , the inertia tensor along the principal axis \hat{I}_i and the rotation matrix converting a vector from the inertial into the body fixed frame Λ_i^{-1} . The utilized contact forces as well as the applied rolling friction model are presented in [8]. The non-spherical particles employed in this study are modelled with a multi-sphere approach. Here, spheres of different sizes are merged to form a cluster to accurately approximate complex particle shapes [10]. The general contact force laws remain equal to the ones used for spherical particles [11].

The compressed air nozzles used to separate undesired particles from the material stream are modelled with Computational Fluid Dynamics (CFD), solving the Navier Stokes equation based on a Finite Volume Method. This is achieved with the help of a detailed and locally refined hexagonal cell mesh. Both the fluid field as well as the enclosed nozzle are considered. The equation of continuity and the equation of momentum are solved

$$\frac{\partial \rho_f}{\partial t} + \nabla(\rho_f \vec{u}_f) = 0, \quad (3)$$

$$\frac{\partial(\rho_f \vec{u}_f)}{\partial t} + \nabla(\rho_f \vec{u}_f \vec{u}_f) = -\nabla p + \nabla(\bar{\tau}) + \rho_f \vec{g}, \quad (4)$$

where \vec{u}_f is the fluid velocity, ρ_f the fluid density, p the pressure and $\bar{\tau}$ the fluid viscous stress tensor. The stress tensor can be written as

$$\bar{\tau} = \mu_e [(\nabla \vec{u}_f) + (\nabla \vec{u}_f)^{-1}], \quad (5)$$

where μ_e is the effective viscosity determined from a k- ϵ model, which is widely used to model turbulent gas flows from nozzles [12-14].

To save computational time and due to the short activation duration of the nozzles a “one-way” coupling is performed between CFD and DEM to realize the particle–fluid interaction in the optical sorter. “One-way” coupling means that the fluid field is affecting the particle motion but not vice versa. The fluid velocity is averaged in every CFD cell and the resulting fluid velocity field is transferred to the DEM upon initialization. The particle–fluid force described in eq. (1) equals the sum of all individual particle–fluid forces. A popular model also suitable for complex shaped particles is the approach devised by Di Felice [15], where the respective force reads

$$\vec{F}_i^{pf} = \vec{F}_i^d + \vec{F}_i^{\nabla p} = \frac{1}{2} \rho_f |\vec{u}_f - \vec{u}_p| C_D A_{\perp} \varepsilon_f^{1-\chi} (\vec{u}_f - \vec{u}_p). \quad (6)$$

Here, \vec{F}_i^d is the drag force, $\vec{F}_i^{\nabla p}$ the pressure gradient force, \vec{u}_p the particle velocity, C_D the drag coefficient, A_{\perp} the cross-sectional area perpendicular to the flow, ε_f the local fluid porosity and χ a correction factor. χ is a function of the particle Reynolds-number

$$Re = \varepsilon_f \rho_f d_p |\vec{u}_f - \vec{u}_p| / \mu_f \quad (7)$$

and is calculated as

$$\chi = 3.7 - 0.65 \exp\left(-\frac{(1.5 - \log(Re))^2}{2}\right), \quad (8)$$

where d_p is the particle diameter and μ_f the fluid viscosity. The drag coefficient is derived from a correlation proposed by Hölzer and Sommerfeld [16] and is written as

$$C_D = \frac{8}{Re} \frac{1}{\sqrt{\phi_\perp}} + \frac{16}{Re} \frac{1}{\sqrt{\phi}} + \frac{3}{\sqrt{Re}} \frac{1}{\phi^{3/4}} + 0.42 \times 10^{0.4(-\log(\phi))^{0.2}} \frac{1}{\phi_\perp}, \quad (9)$$

where ϕ_\perp is the crosswise sphericity, which is defined as the ratio between the cross-sectional area of a volume equivalent sphere and the projected cross-sectional area of the considered particle perpendicular to the flow. ϕ is the sphericity, namely the ratio between the surface area of a volume equivalent sphere and the surface area of the particle considered.

2.2 Experimental and numerical setup

A modular optical belt sorter is used to conduct the experiments presented and as a baseline for the numerical model and the simulations performed. The modular optical belt sorter combines all major components of a regular full size sorter with the advantage of being easy to adjust, handle and operate. The experimental and numerical setup is shown in Figure 1. Both setups consist of a vibrating feeder, a conveyor belt and the particle separation stage with compressed air nozzles, as well as a separation container. The vibrating feeder operates at a frequency of 50 Hz and at an angle of 25° . The amplitude of the feeder can be regulated. The conveyor belt runs at a constant velocity of 1.1 m/s and a total of sixteen air nozzles are employed for particle ejection.

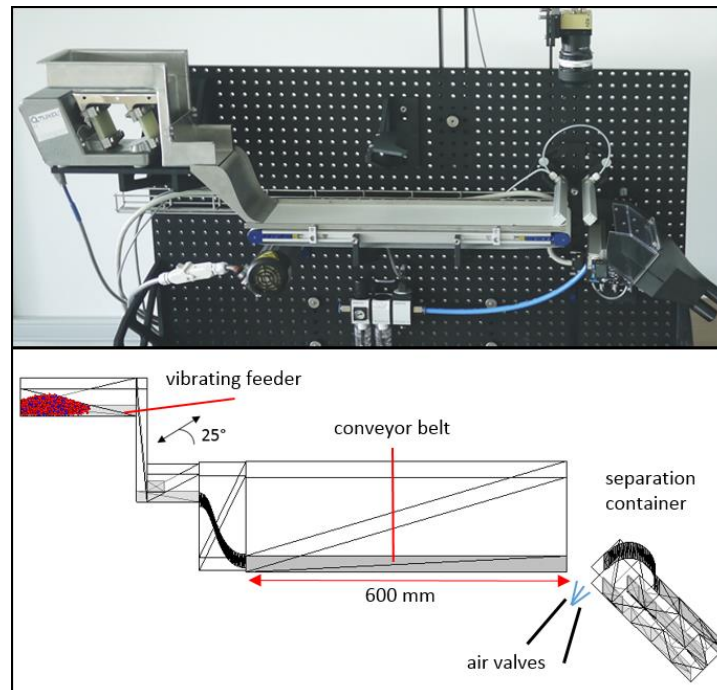


Figure 1: Experimental (top) and numerical (bottom) setup of the optical belt sorter

The sorting task in both the experiment and the simulation is to separate 10 g of colored peppercorns from 40 g of uncolored ones in batch operation. At the start of the process, the two particle fractions are mixed and a total of 50 g of peppercorns are randomly filled in a container, which is then placed on top of the already vibrating feeding system. The container is lifted and the particles are transported towards the conveyor belt by a slide. In the experimental investigation a line scan camera is located at the end of the belt. The color of passing particles is detected and depending on the y-location of the peppercorn, a specific nozzle is activated. The delay between particle detection and nozzle activation is calculated by assuming that the particle is moving with belt velocity. Particle movement orthogonal to the belt is neglected.

2.3 Investigated bulk solids and DEM operating parameters

The bulk solids chosen for the presented study are green peppercorns. They are selected due to their easy accessibility, importance in the optical sorting industry and irregular movement on the conveyor belt. The latter makes the sorting task especially difficult and allows a detailed analysis of the influence of different operational parameters.

In order to determine the particle properties and to model the peppercorns within the DEM a size, volume and density investigation is conducted. Based on a shadow projection of different peppercorns, five particle shape types are created using particle clusters. The approximation is performed with a MATLAB script by filling the depicted particle outline with 8–10 spheres, depending on the complexity of the shape. This can be seen in Figure 2. A volume-based size distribution with five different particle sizes is implemented to ensure a correct representation of the packing structure and local solid fraction distribution within a particle packing and therefore the overall approximation quality.

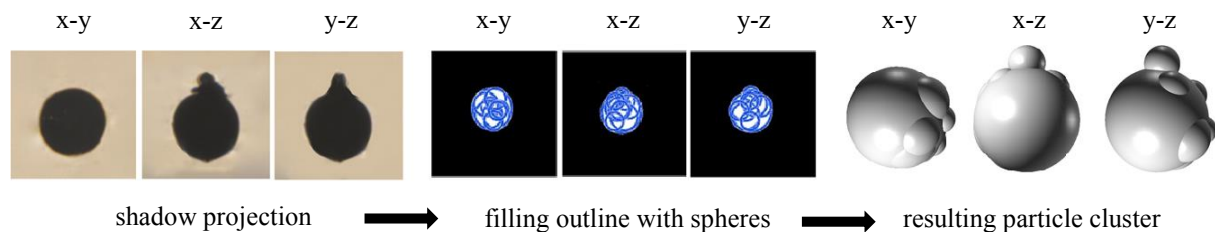


Figure 2: Peppercorn approximation for the DEM

Apart from the particle shape and size, important DEM parameters describing the particle–particle as well as particle–wall interaction have to be defined. The coefficients of normal restitution, Coulomb friction and rolling friction are initially determined experimentally on a single particle scale according to the procedures described by Höhner et al. [17] and Sudbrock et al. [18]. For the particle–wall contacts, the steel used for the vibrating feeder and slide of the sorter and the material of the conveyor belt are considered.

In order to optimize the resulting parameters, further tests are conducted and compared between experiments and simulation. To analyze the parameters in a dynamic scenario, a rotary drum with a steel/belt material outline is filled with peppercorns to account for one third of the drum volume. The drum is then rotated with a constant velocity and the resulting angle of repose is compared between simulation and experiment. A comparison can be seen in Figure 3.

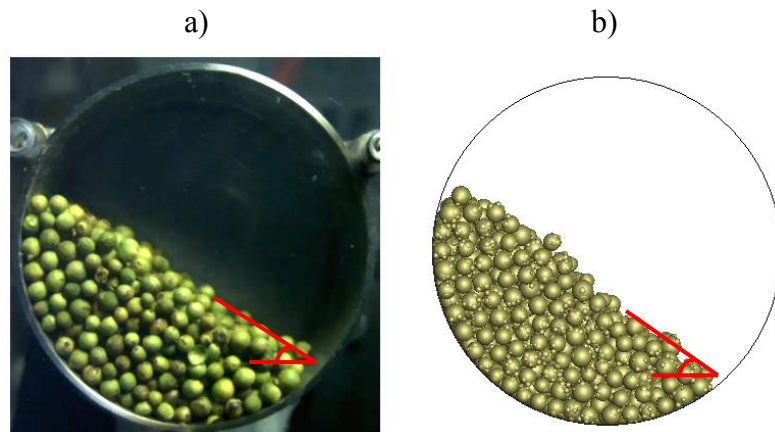


Figure 3: Angle of repose compared between a) experiment and b) simulation, dynamic scenario

In a second step, a static scenario is investigated, where a defined mass of peppercorns is filled into a stationary cylinder. The cylinder was previously placed on a steel/belt material base. Once the particles settle, the cylinder is lifted upwards with a defined velocity and the particles form a pile on the respective surface material. A second, wider ring prevents the almost spherical peppercorns from rolling off the test rig. Similar to the dynamic investigation the resulting angle of repose is compared between simulation and experiment, see Figure 4. Both sides of the pile are considered and the two angles are combined to calculate a total angle of repose.



Figure 4: Angle of repose compared between a) experiment and b) simulation, static scenario

After comparing the angles between the experiment and the simulation, the initial DEM particle parameters are slightly adjusted and another dynamic and static simulation is performed. The established angles are compared again and the process is repeated until the parameters employed result in matching angles of repose both for the static and dynamic scenario. The final particle parameters for the peppercorns are presented in Table 1. The rolling friction coefficient is considered to be equal for all contact forms.

Table 1: Particle properties of the peppercorns required for them DEM simulations

Particle property	Value
Average mass [g]	0.0271
Average density [kg/m ³]	551.47
Restitution coefficient PP [-]	0.627
Restitution coefficient PW sorter [-]	0.721
Restitution coefficient PW belt [-]	0.701
Friction coefficient PP [-]	0.4
Friction coefficient PW sorter [-]	0.326
Friction coefficient PW belt [-]	0.336
Rolling friction coefficient [-]	0.00008

The DEM simulations are performed with a time step of $1 \cdot 10^{-5}$ s and a maximum particle overlap of 0.5 % of the particle diameter is ensured. The spring stiffness k^n and k^t as well as the damping coefficient γ^n are calculated from the chosen time step and the respective coefficient of restitution.

2.4 Air nozzle model and implementation within the numerical setup

To simulate the fluid flow within the air nozzle and in the resulting flow field forming at the nozzle outlet, a hexagonal mesh of the air nozzle interior and the adjacent airspace is created. A CAD model of the nozzle bar employed in the modular optical belt sorter (Figure 5 a) is used for generating the basic nozzle geometry, see Figure 5 b). Only one of the sixteen nozzles is utilized. The nozzle has one inlet and splits up into four nozzle outlets to cover the entire width of the conveyor belt.

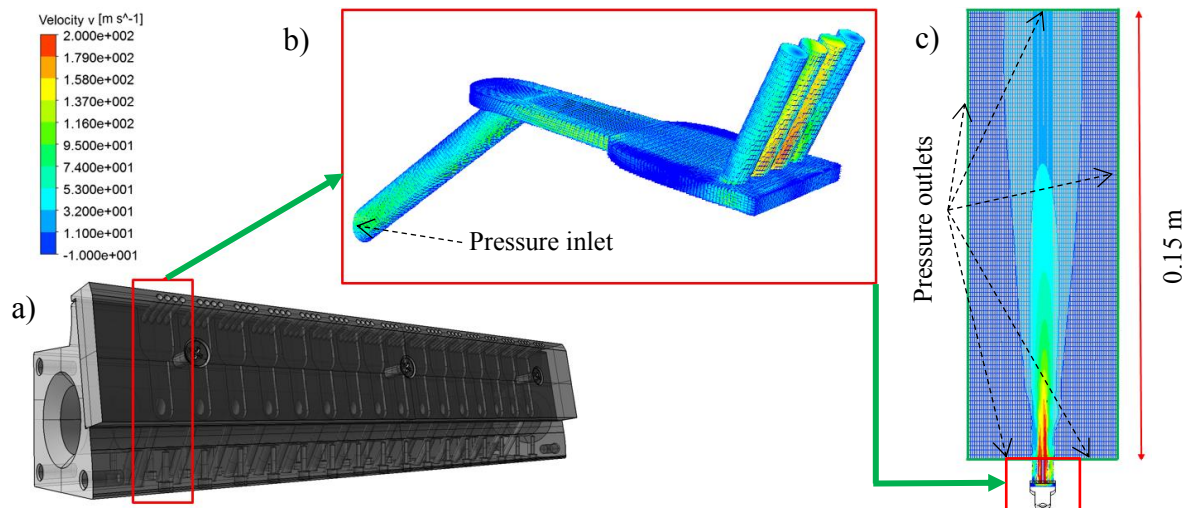


Figure 5: Air nozzle mesh b) derived from a CAD model of the sorting system nozzle bar a) and resulting fluid field c)

A pressure inlet is defined at the nozzle inlet and pressure outlets at the outer edges of the modelled airspace, see Figure 5 c). A gauge pressure of 1.25 bar is applied at the pressure inlet and the adjacent room is filled with quiescent air. The calculation is performed stationary and the fluid is assumed as incompressible. A standard k - ϵ turbulence model is employed. The air has a density of $\rho_f = 1.225 \text{ kg/m}^3$, viscosity of $\mu_f = 1.7894 \cdot 10^{-5} \text{ kg/(m}\cdot\text{s)}$ and a temperature of $T_f = 293.15 \text{ K}$.

Once the CFD calculation has converged, the resulting fluid data is prepared for utilization within the DEM. As the resolution of the fluid grid is very fine with 1.86 million cells and would result in very long simulation durations when used in the DEM, the fluid properties are averaged to larger cells. In addition, the fluid field is trimmed to fit the air jet contours, which also reduces the amount of fluid cells and therefore the required calculation time. The new fluid cells have a dimension of $2 \times 2 \times 2 \text{ mm}^3$ and cover a volume of $20 \times 50 \times 150 \text{ mm}^3$. To model the entire nozzle bar, the fluid cell zone calculated for a single nozzle is duplicated sixteen times and joint together to form one large grid, now consisting of 159,375 cells.

When a particle enters the zone where the fluid cells are coupled with the DEM, the fluid properties of every fluid cell that lies within the particle boundary are averaged and used to calculate the particle–fluid force described in Section 2.1. If a particle enters a zone in which the fluid fields of two nozzles overlap, there are three different possibilities regarding which fluid properties are assigned to the fluid cells and used for calculation. Depending on the nozzles activated by the prediction algorithm at the particle detection stage, either nozzle 1, nozzle 2 or both nozzles are activated. In the first two cases, the fluid properties of the respective nozzle are considered. If both are activated, the fluid properties of the nozzle with the higher absolute velocity at the cell position are assigned to the fluid cell.

3 RESULTS AND DISCUSSION

3.1 Comparison of mass flow between experiment and simulation

To ensure that the particle approximation as well as the determined particle parameters are correct and suitable to model the particle behavior within the optical sorter, the mass flow of peppercorns is measured both experimentally and numerically. As the mass flow rate is highly dependent on the vibrating feeder amplitude, a high-speed camera is used to analyze the amplitude, angle and frequency of the induced vibration in detail. Results show that the frequency and vibration–angle are constant with values of 50 Hz and 25° respectively. The amplitude can be regulated with a transformer and three amplitudes of $a_1 = 0.402 \text{ mm}$, $a_2 = 0.278$ and $a_3 = 0.236$ were measured and then used for the comparison.

To measure the exiting particle mass flow in the experimental setup, a scale with a collecting container is positioned at the end of the conveyor belt and connected to a computer. Both the air nozzles as well as the separation container are removed during the procedure. At the start of the experiment, the same procedure used for the separation investigation described in Section 2.2 is employed. 100 g of peppercorns are used in all iterations and the measurement is repeated three times for each investigated amplitude setting. The results are shown in Figure 6.

The figure shows that there is good agreement between the DEM simulations and the conducted experiments. Slight offsets can be seen at the end of the process, especially for small amplitudes. Here, the peppercorns in the simulation exit the system at a faster pace. Further

investigation showed that this is likely due to small irregularities and dents on the surface of the vibrating feeder of the experimental setup. These imperfections cause particle movement to slow down, especially when the peppercorns no longer move in bulk.

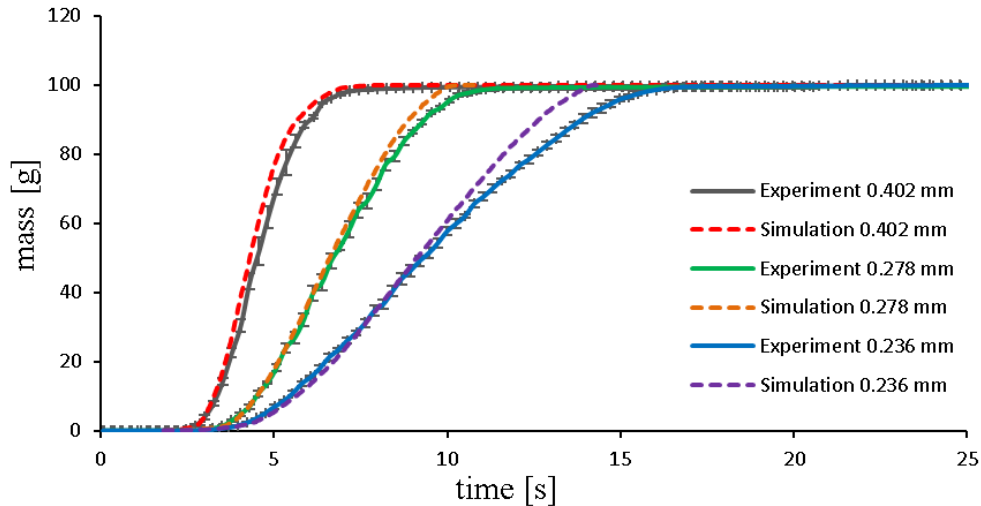


Figure 6: Exiting mass of peppercorns for different operating amplitudes compared between experiment and simulation

3.2 Comparison of separation results

For both the experimental and numerical investigation of particle separation, the operation procedure described in Section 2.2 is applied. The experiment is carried out first and important system parameters vital for efficient particle separation like valve activation duration, distance between particle detection and separation stage, applied nozzle gauge pressure and orientation of the separation container are defined and noted for the DEM–CFD Simulations. It is important to keep in mind that the goal of the conducted experiment is not to achieve a perfect separation quality, but to ensure that defined system parameters are used that can be transferred to the numerical setup. The system was deliberately run under difficult operating conditions and with a high particle feed rate in order to properly test the numerical accuracy. The experiment is conducted three times.

After the sorting process is complete, the peppercorns are extracted from the separation container and the separation quality is assessed by weighing the different particle fractions. This is of course not necessary for the simulation where the sorting result is directly written to a text file.

The findings of the conducted experimental and numerical sorting process and its comparison are presented in Figure 7. The error bars represent the standard deviation of the three conducted experiments. The results show that there is generally good agreement between the experiment and simulation. Figure 7 a) shows the percentage of the colored peppercorns ejected and not ejected from the material stream. The amount of particles ejected is only slightly higher for the simulation, which is most likely due to the fact that a small amount of particles is not correctly identified by the line scan camera. This is of course not the case in the

simulation. The separation results of the uncolored particles can be seen in Figure 7 b). Only a small amount of by-catch is produced and the simulation differs from the results obtained from the experiment only by a very small margin. The percentage of missing particles (particles that wrongly exit the sorting process, mostly at the separation stage) is shown in Figure 7 c). Here, the percentage of missing particles is significantly higher for the simulation compared to the experimental results. However, as already very few particles have a very high impact on this result and the standard deviation of the three experiments is fairly high, additional simulations and evaluation need to be performed.

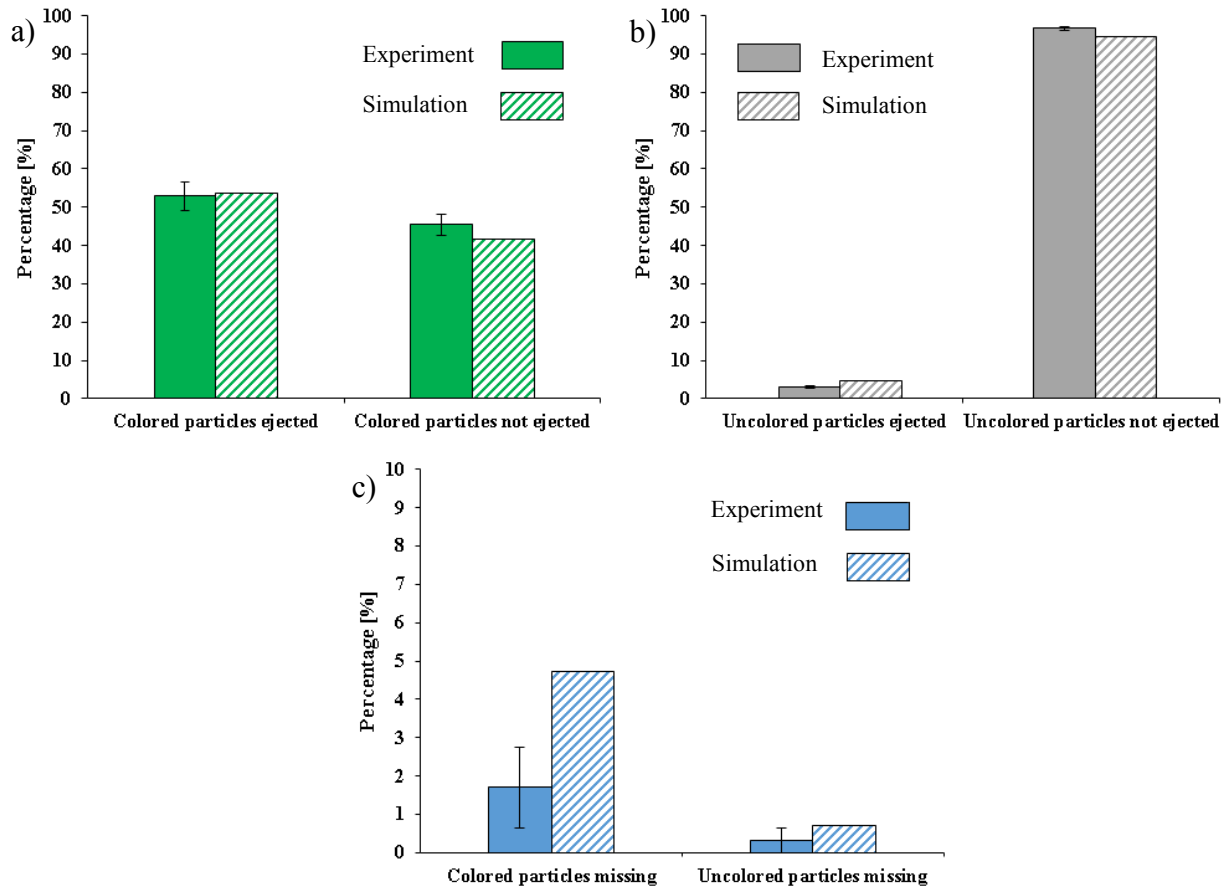


Figure 7: Comparison of particle separation results between experiment and simulation for a) ejected/not ejected colored particles, b) ejected/not ejected uncolored particles and c) colored/uncolored missing particles

4 CONCLUSION

A fully automated optical belt sorter was numerically modelled with a coupled DEM–CFD approach. Complex shaped particles were approximated with the help of particle clusters and DEM parameters were derived by experimental and numerical investigations. Particle mass flow through the optical sorter was analyzed for different vibrating feeder amplitudes in matching numerical and experimental setups. The compressed air nozzles of the sorter were modelled with CFD and the resulting fluid field coupled with the DEM upon initialization in a “one–way” coupling approach. An experiment with a defined sorting task was conducted on

the modular sorting system and separation results were compared to those of corresponding DEM–CFD simulations.

- The particle approximation of peppercorns by particle clusters and the DEM parameter definition shows good results when comparing the particle mass flow through the sorter between experiment and simulation. At low vibrating feeder amplitudes, the simulation shows a slightly higher mass flow rate compared to experimental findings, which is most likely explained by small imperfections on the surface of the vibrating feeder, causing the peppercorns' velocity to slow down.
- The comparison of the separation results shows good agreement between conducted DEM–CFD simulations and experiments. The presented modelling approach seems promising and suitable for further investigation.
- Additional research analyzing different operating parameters of the optical sorter is planned, where other particles like maize grains or coffee beans are employed. Altering other important system parameters like material composition, valve activation duration or conveyor belt velocity is also planned for future investigation.

Acknowledgement

The IGF project 18798 N of the research association Forschungs–Gesellschaft Verfahrens–Technik e.V. (GVT) was supported via the AiF in a program to promote the Industrial Community Research and Development (IGF) by the Federal Ministry for Economic Affairs and Energy on the basis of a resolution of the German Bundestag.

REFERENCES

- [1] Duran, J. *Sands, Powders and Grains*. Springer New York, (2000).
- [2] Stieß, M. *Mechanische Verfahrenstechnik I*. Springer Berlin, (1995).
- [3] McGlichey, D. *Characterisation of Bulk Solids*. Blackwell Publishing Ltd. Oxford, (2005).
- [4] De Jong and Harbeck, T.P.R. Automated sorting of minerals: current status and future outlook. *Proc. 37th Can. Miner. Process. Conf.* (2005) 629-648.
- [5] Pascoe, R.D., Udoudo, O.B. and Glass H.J. Efficiency of automated sorter performance based on particle proximity information. *Miner. Eng.* (2015) **23**:806-812.
- [6] Pascoe, R.D., Fitzpatrick, R. and Garratt, J.R. Prediction of automated sorter performance utilizing a Monte Carlo simulation of feed characteristics. *Miner. Eng.* (2015) **72**:101-107.
- [7] Fitzpatrick, R.S., Glass H.J. and Pascoe R.D. CFD–DEM modelling of particle ejection by a sensor–based automated sorter. *Miner. Eng.* (2015) **79**:176-184.
- [8] Pieper, C., Maier, G., Pfaff, F., et al. Numerical modeling of an automated optical belt sorter using the Discrete Element Method. *Powder Technol.* (2016) **301**:805-814.
- [9] Cundall, P.A. and Strack, O.D.L. A discrete numerical model for granular assemblies. *Geotechnique* (1979) **29**:47-65.
- [10] Kruggel-Emden, H., Rickelt, S., Wirtz, S. and Scherer, V. A study on the validity of the multi–sphere discrete element method. *Powder Technol.* (2008) **188**:153-165.
- [11] Höhner, D., Wirtz, S., Kruggel-Emden, H. and Scherer, V. Comparison of the multi-sphere and polyhedral approach to simulate non-spherical particles within the discrete

- element method: influence of temporal force evolution for multiple contacts. *Powder Technol.* (2011) **208**:643-656.
- [12] Xue, K., Li, K., Chen, W., Chong, D. and Yan, J. Numerical investigation on the performance of different primary nozzle structures in the supersonic ejector. *Energy Procedia* (2017) **105**:4997-5004.
- [13] Raj, A.R.G.S., Mallikarjuna, J.M. and Ganesan, V. Energy efficient piston configuration for effective air motion – A CFD study. *Applied Energy* (2013) **102**:347-354.
- [14] Chu, H., Zhang, R., Qi, Y. and Kann, Z. Simulation and experimental test of waterless washing nozzles for fresh apricot. *Biosystems Engineering* (2017) **159**:97-108.
- [15] Di Felice, R. The voidage function for fluid–particle interaction systems. *Int. J. Multiph. Flow* (1994) **20**:153-159.
- [16] Hölzer, A. and Sommerfeld, M. New simple correlation formula for the drag coefficient of non-spherical particles. *Powder Technol.* (2008) **184**:361-365.
- [17] Höhner, D., Wirtz, S. and Scherer, V. Experimental and numerical investigation on the influence of particle shape and shape approximation on hopper discharge using the discrete element method. *Powder Technol.* (2013) **235**:614-627.
- [18] Sudbrock, F., Simsek, E., Rickelt, S., Wirtz, S. and Scherer, V. Discrete element analysis of experiments on mixing and stoking of monodisperse spheres on a grate. *Powder Technol.* (2011) **208**:111-120.